

Enhancement of the Josephson critical current in a multiterminal SINIS device under current injection

I. P. Nevirkovets,^{1,2} S. E. Shafranuk,¹ O. Chernyashevskyy,^{1,2} and J. B. Ketterson^{1,3}

¹*Department of Physics and Astronomy, Northwestern University, Evanston, Illinois 60208, USA*

²*Institute for Metal Physics, NASU, 03680 Kyiv, Ukraine*

³*Department of Electrical Engineering and Computer Science and Materials Research Center, Northwestern University, Evanston, Illinois 60208, USA*

(Received 20 June 2007; revised manuscript received 29 August 2007; published 28 November 2007)

In a multiterminal SINIS (Nb/Al/AIO_x/Al/AIO_x/Al/Nb) device (where S, I, and N denote a superconductor, insulator, and normal metal), which has electrical leads connected to the middle N (Al) layer, a current passing through one of the subjunctions (NIS) modulates the supercurrent through the other subjunction (SIN), so that, at some injection levels, the supercurrent increases above its steady state value. A theoretical model is given that describes the effect in terms of nonlinear coupling of the two subjunctions due to the electric current controlled by the proximity effect in the N layer.

DOI: 10.1103/PhysRevB.76.184520

PACS number(s): 74.45.+c, 74.50.+r, 74.78.Fk, 85.25.Am

I. INTRODUCTION

Systems composed of strongly coupled Josephson junctions are commonly used as the active elements in superconducting electronics,^{1,2} including qubit circuits.³ In our former works, we have demonstrated the feasibility of a multiterminal device based on an *in situ* deposited SINIS structure, where electrical contact is made to two exposed regions of a thin N film; here S, I, and N denote a superconductor (Nb), an insulator (AIO_x), and a normal metal (Al), respectively.⁴⁻⁶ In the device, the bottom SIN and top NIS junctions are strongly coupled via the common thin N layer to form a single Josephson junction. The multiterminal geometry was used to probe the nonequilibrium and proximity effects in the weak-link region of a Josephson SINIS junction; a striking anisotropy in the electrical transport through the N layer was found, and the nature of some anomalous features in the conductivity of the SINIS junctions was studied.⁴⁻⁶ The multiterminal devices may have potential for application in a qubit gate and as an active element of the ordinary superconducting electronics. Experimental observation of current and power amplification using the quasiparticle characteristics of such devices has been reported.⁴

Here we study the influence of the injection current through one NIS subjunction (the top) on the Josephson current through a second NIS subjunction (the bottom). Although we are nominally dealing with SIN junctions, in a strongly coupled SINIS structure, they display a zero-voltage Josephson current, if a bias current flows across either one barrier or both barriers simultaneously; on the other hand, the current-voltage characteristic (CVC) of the middle Al layer measured in the lateral direction displays a *dissipative* conductivity.⁵ This can be explained by a theoretical model,^{3,7} according to which the supercurrent across the whole SINIS junction is carried via the Andreev bound states.^{8,9} These states^{8,9} arise from a quantum interference between the wave functions of the electrons and holes, which move in opposite directions. Because in a sandwich-type SINIS junction the quantization occurs in the direction perpendicular to the barriers, the supercurrent through the middle N

layer is essentially one dimensional. Since there is no quantization in the lateral direction (parallel to the barriers), the lateral conductivity of the N layer is dissipative. This may lead to some nonequilibrium effects in the N layer while the current is flowing through it. Here, we neglect such nonequilibrium effects and show that the observed phenomena, specifically, Josephson critical current enhancement in the bottom SIN subjunction and its CVC shift along the current axis in the presence of the current injection through the top NIS subjunction, can be qualitatively explained by current-controlled proximity interaction between the subjunctions.

II. EXPERIMENTAL RESULTS

The fabrication as well as the basic properties of our multiterminal Nb/Al/AIO_x/Al/AIO_x/Al/Nb devices have been discussed elsewhere.⁴⁻⁶ The devices described here had a width $W=10\ \mu\text{m}$ and lengths $L_1=19\ \mu\text{m}$ and $L_2=11\ \mu\text{m}$ for the bottom and top subjunctions, respectively [a schematic of the device configuration is shown in the inset of Fig. 1(a)]; the thickness of the middle Al layer, d_N , is nominally 16 nm. All characteristics described here were measured at 1.8 K.

First, we consider the unperturbed CVC of the bottom and top subjunctions, $I_1(V_1)$ and $I_2(V_2)$ [see Figs. 1(a) and 1(b), respectively]. The shape of the CVC depends on the measurement configuration. For the same current path, the voltage can be measured in two ways, as shown in the insets to Figs. 1(a) and 1(b), i.e., the voltages $V_1^{(2)}$ and $V_2^{(2)}$ include a contribution from resistance of the Al film, whereas the voltages $V_1^{(1)}$ and $V_2^{(1)}$ do not. Only in the second case [curves $I_1(V_1^{(1)})$ and $I_2(V_2^{(1)})$] does the CVC display a zero-voltage Josephson branch; in curves $I_1(V_1^{(2)})$ and $I_2(V_2^{(2)})$ these Josephson branches are tilted, following the shape of the resistive background.

In the experiment, we studied how an injection current through the top subjunction, I_2 , modifies the $I_1(V_1^{(1)})$ curve of the bottom subjunction, as illustrated in Fig. 2, and modulates the apparent Josephson critical current, I_{c1} (see Fig. 3). In Fig. 2, the CVC of the bottom junction is shown for I_2

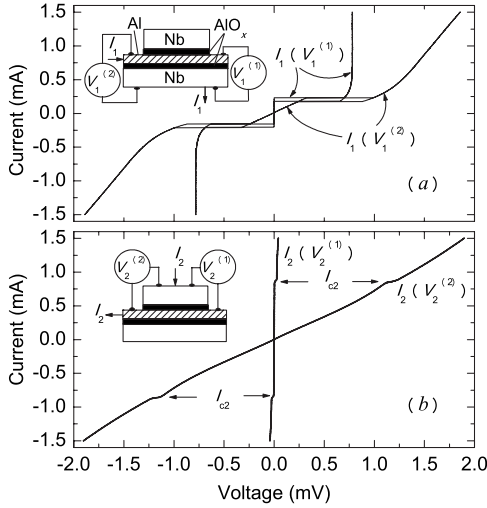


FIG. 1. Current-voltage characteristic (CVC) of the bottom (a) and top (b) junctions, $I_1(V_1)$ and $I_2(V_2)$, respectively, at $T=1.8$ K. Different modes of voltage measurement are shown in the insets.

$= +1.2$ mA for zero applied magnetic field H (solid curve 1), and for a magnetic field of 51 Oe applied parallel to the junction plane (dotted curve 2); curve 3 is the unperturbed CVC, and curve 4 is for $I_2 = -1.5$ mA (curves 3 and 4 are for $H=0$). Here, the $+$ direction of the injection current I_2 corresponds to the current configuration shown in the inset of Fig. 2. One can see a significant increase of the Josephson critical current I_{c1} in curves 1 and 4 as compared with I_{c1} for the unperturbed curve 3. The increase occurs in the presence of both dissipative current through the Al film and superconducting current across the tunnel barriers and through the Nb electrodes. Ramping the current I_1 in the presence of the injection current I_2 leads to a complex interaction of the two junctions; as a result, their critical currents I_{c1} and I_{c2} lock to each other, and the junctions switch to the resistive state

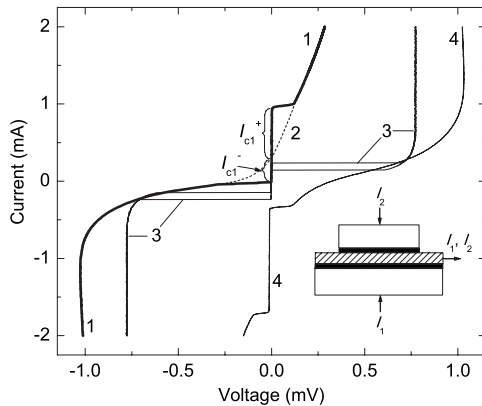


FIG. 2. Current-voltage characteristic (CVC) of the bottom junction for $I_2 = +1.2$ mA in zero applied magnetic field H (curve 1), and for a magnetic field of 51 Oe applied parallel to the junction plane (curve 2); curve 3 is the unperturbed CVC, and curve 4 is for $I_2 = -1.5$ mA (both curves are for $H=0$). The $+$ direction of the injection current I_2 corresponds to the current configuration shown in the inset. $T=1.8$ K.

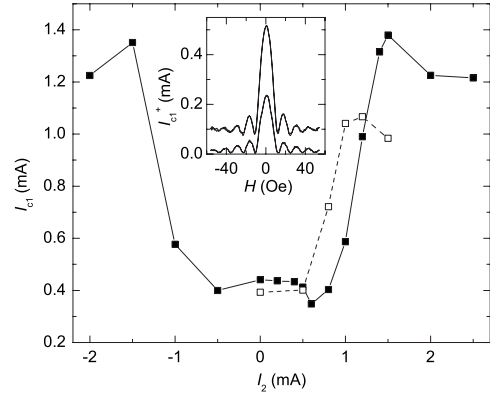


FIG. 3. Josephson critical current of the bottom junction as a function of the injection current through the top junction for two devices with nominally identical parameters at 1.8 K. For one of the devices, the inset shows I_c vs H dependence for the unperturbed bottom junction (lower curve) and for the same junction at $I_2 = 1$ mA (upper curve). The last curve is shifted downward along the current axis by 0.6 mA for better clarity.

simultaneously.⁵ At some level of the injection current I_2 , the CVC of the bottom junction shifts along the current axis, so that one may have an unusual situation (shown in Fig. 2) where the Josephson current is flowing in one direction (positive or negative, depending on the I_2 direction) for both positive and negative voltages. Importantly, not only does the injection current enhance the Josephson current of the bottom junction, but it also dramatically modifies the quasiparticle branch of the CVC (see also Ref. 4), indicating strong nonequilibrium caused by injection.

In Fig. 3, we plot the dependence of the Josephson critical current of the bottom junction, I_{c1} , as a function of the injection current through the top junction, I_2 , for two devices with nominally identical parameters. Here, I_{c1} denotes the sum of the Josephson critical currents I_{c1}^+ and I_{c1}^- above and below the point $I_1=0$, respectively (cf. Fig. 2). Note the nonmonotonic dependence of I_{c1} on I_2 : initially, I_{c1} grows with I_2 , reaches a maximum, and then decreases. The diffraction pattern for the Josephson current (measured only for the upper branch $I_{c1}^+ > 0$) is shown in the inset of Fig. 3 for $I_2=0$ (lower curve) and $I_2=1$ mA (upper curve; offset for clarity by 0.6 mA along the current axis). This dependence demonstrates good junction quality and the Josephson nature of the stimulated current (for $I_2 \neq 0$). In general, the stimulated currents I_{c1}^+ (for $I_1 > 0$) and I_{c1}^- (for $I_1 < 0$) may be not equal to each other (cf. Fig. 2), and their diffraction patterns may deviate substantially from the $I_c(H)$ dependence of an ideal Josephson junction (with $I=I_c \sin \varphi$, where φ is the phase difference); this issue will be considered in more detail elsewhere. Here, we focus on the physical origin for the Josephson current stimulation in our system, as outlined in the theoretical model presented below.

III. THEORETICAL MODEL AND DISCUSSION

We emphasize that despite the dissipative conductivity of the N layer, the x component of the electric current (perpen-

dicular to the barriers) has purely a Josephson nature. This occurs because the amplitude of the superfluid condensate wave function induced by the proximity effect in N is finite,¹⁰ although the superconducting energy gap vanishes. The proximity-induced superconductivity in N is purely one dimensional. Therefore, in the x direction, the SINIS junction may be treated as a system of two strongly interacting SIN (bottom) and NIS (top) Josephson subjunctions J_1 and J_2 , respectively, coupled by their common N layer. This approximation of the SINIS system allows us to explain the two main experimental facts. (a) The absolute value of the partial critical supercurrent $I_{c1} = I_{c1}^+ + |I_{c1}^-|$ of the subjunction J_1 may considerably increase under influence of a finite bias supercurrent $I_2 \neq 0$ (fed through the adjacent subjunction J_2) as compared to its unperturbed value I_{c1}^0 (corresponding to $I_2 = 0$). Here the index 1 (2) corresponds to the bottom (top) subjunction; $I_{c1}^{+(-)}$ is the upper (lower) value of the partial critical supercurrent, as explained above (cf. Fig. 2). (b) At some level of $I_2 < 0$, when recording the CVC $I_1(V_1)$ of the junction J_1 , one reaches the resistive state of J_1 . This resistive state is unusual: the voltage V_1 may become negative, although the bias current I_1 is positive ($I_1 > 0$). Except for this feature, for the sake of simplicity, here we do not discuss the properties of the resistive state at a finite bias voltage; also, we do not consider the associated nonequilibrium effects.

The experimental behavior described above may be understood within a model of two strongly interacted Josephson junctions, developed in Ref. 3 (see also references therein). According to the model,³ the subjunctions J_1 and J_2 are coupled to each other due to the superconducting proximity effect described in terms of elementary Andreev reflection processes. The same mechanism is responsible for the Josephson supercurrent across the subjunctions J_1 and J_2 . The phenomena discussed may be illustrated for the case of weakly coupled subjunctions, where one may write for the total energy of the SINIS junction:

$$W_{12} \simeq W_1^{(0)} + W_2^{(0)} + U_{12}, \quad (1)$$

where $W_{1,2}$ is the energy of a dc-current-biased single non-interacting Josephson junction, and U_{12} is the interaction energy. The energy $W_{1,2}$ is

$$W_{1,2}^{(0)} = \frac{\Phi_0}{2\pi} [I_{c1,2}(1 - \cos \varphi_{1,2}) - I_{1,2}\varphi_{1,2}], \quad (2)$$

where $I_{c1,2}$ is the partial Josephson critical current for a non-interactive subjunction $J_{1,2}$, Φ_0 is the flux quantum. The Josephson potential energy (2) is quoted as a ‘‘washboard,’’ whose tilting with respect to the $\varphi_{1,2}$ axes is controlled by $I_{1,2}$ (see, e.g., Ref. 11). A simplified expression for the interaction term U_{12} is

$$U_{12} = \zeta \cos(\varphi_2 - \varphi_1), \quad (3)$$

where ζ is the coupling parameter (here we assume $\zeta \ll 1$). The interaction term described by Eq. (3) depends on the partial phase differences φ_1 and φ_2 across the subjunctions J_1 and J_2 . We emphasize that the intrinsic interaction (3) yields additional nonlinear terms in the partial Josephson currents. An electromagnetic interaction linear in Josephson current

between adjacent SIS junctions is studied in Ref. 12; this kind of interaction does not lead to the Josephson current enhancement described here. A nonlinear interaction term similar to that given by Eq. (3) was phenomenologically introduced by Carapella *et al.*¹³ to describe Josephson coupling in a SISIS stack with a thin middle S layer; the authors¹³ found the possibility of the supercurrent enhancement in the stack and appearance of the half-integer Shapiro steps. In our case, the nonlinear interaction constant ζ entering Eq. (3) is computed microscopically using the approach.³ The constant ζ depends on the junction transparency D , the thickness of the middle N layer, its purity, and material properties of the S electrodes.

The phase differences φ_1 and φ_2 for given bias currents I_1 and I_2 are obtained from Eqs. (1) and (2) using the condition

$$\frac{\partial W_{12}(\varphi_1, \varphi_2)}{\partial \varphi_{1,2}} = 0. \quad (4)$$

For decoupled junctions ($\zeta = 0$), on the assumption that $I_{1,2} < I_{c1,2}$, Eq. (4) gives the well-known Josephson relationship $I_{1,2}(\varphi_{1,2}) = I_{c1,2} \sin \varphi_{1,2}$, providing that $I_{c1,2}^{\pm} = \pm I_{c1,2}$. The Josephson junction switches into the resistive state when $I_{1,2} \geq I_{c1,2}$. The last condition is strongly affected by the interaction between the J_1 and J_2 subjunctions. Using Eqs. (1), (2), and (4) at $\zeta \neq 0$, one gets a more complicated current-phase relationship:

$$I_{1,2}(\varphi_{1,2}) = I_{c1,2}(1 - \zeta \cos \varphi_{2,1}) \sin \varphi_{1,2} + \zeta \cos \varphi_{1,2} \sin \varphi_{2,1}. \quad (5)$$

One can see that the current-phase relationship (5) for junctions J_1 and J_2 is modified by the interjunction interaction ($\zeta \neq 0$), while the critical current is renormalized as $I_{c1,2} \rightarrow I_{c1,2}(1 - \zeta \cos \varphi_{2,1})$. This means that the critical current of each subjunction may be either increased or suppressed by the factor of $(1 - \zeta \cos \varphi_{2,1})$. The renormalization is controlled by the bias current $I_{2,1}$ flowing across the adjacent subjunction $J_{2,1}$. In particular, at $\varphi_{2,1} = 0$, the partial critical current $I_{c1,2}$ decreases, while at $\varphi_{2,1} = \pi$ it increases. One can also see an asymmetric change of the upper and lower partial critical currents $I_{c1,2}^{\pm} \simeq \pm I_{c1,2}(1 - \zeta_1 \cos \varphi_{2,1}) + \zeta_2 \sin \varphi_{2,1}$, where $(\zeta_1 + \zeta_2)/2 = \zeta$ and $|\zeta_1 - \zeta_2| \neq 0$ due to the asymmetry of the subjunctions. More accurate consideration requires numerical computation of the current-phase relationship for given trajectories of the system, and of the corresponding CVC. Both of the mentioned effects (i.e., the renormalization of $I_{c1,2}$ and the asymmetric change of $I_{c1,2}^{\pm}$) are caused by the interjunction interaction across the common N layer. The interaction constant ζ is computed microscopically as described earlier (see, e.g., Ref. 3 and references therein).

In the strong coupling limit (which is the case in the experiment described above) a simple analytical expression for the critical current change, δI_c , caused by injection, is not available. Therefore the problem is solved numerically. The local supercurrent across each of the subjunctions is computed using the quasiclassical Green function approach.³ The coupling energy between the subjunctions J_1 and J_2 is then given by

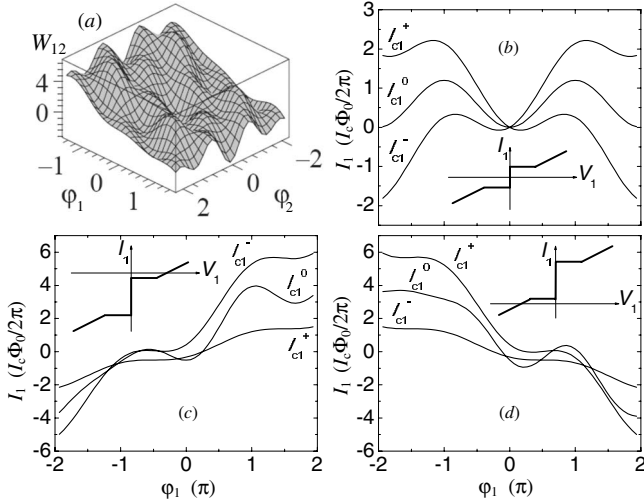


FIG. 4. (a) Josephson energy $W_{1,2}(\varphi_1, \varphi_2)$ for the SINIS junction. (b) Current-phase relationship which corresponds to $I_1 = I_{c1}^+$, $I_1 = I_{c1}^0$, and $I_1 = I_{c1}^-$ in the absence of the bias current through the adjacent junction, $I_2 = 0$. (c) and (d) are the same as (b), but for a finite $I_2 < 0$ and $I_2 > 0$, respectively.

$$U_{12}(\varphi_2) = \max_{\varphi_1} (W_{12} - W_1^{(0)} - W_2^{(0)}), \quad (6)$$

where $W_{12}(\varphi) = \Phi_0 \int_{\varphi_0}^{\varphi} I_s^{(\text{SINIS})}(\varphi') d\varphi' / 2\pi$ and $W_{1,2}^{(0)}(\varphi) = 2\Phi_0 \int_{\varphi_0}^{\varphi} I_{1,2}^{(\text{SIN})}(\varphi') d\varphi' / 2\pi$ are the full energies of the two-junction system including the interaction and without any interaction, respectively, with $I_s^{(\text{SINIS})}$ and $I_{1,2}^{(\text{SIN})}$ being the supercurrent through the whole SINIS junction and the SIN (NIS) junction, respectively (assuming that the subjunctions J_1 and J_2 are identical).

The experimental facts (a) and (b) listed above may be understood from an illustration presented in Fig. 4, where in Fig. 4(a) we plot the Josephson energy potential W_{12} given by Eq. (1). If $\zeta \neq 0$, then W_{12} has a complicated profile, and is tilted with respect to the $\varphi_{1,2}$ axes when the partial bias currents $I_{1,2}$ are applied. The system experiences a motion along complicated trajectories located on the W_{12} surface in the $\varphi_{1,2}$ space. Each trajectory λ corresponds to a certain current-phase relationship $I_1^{(\lambda)}(\varphi_1, \varphi_2)$. The exact trajectory depends on the initial conditions [i.e., on the values of $\varphi_{1,2}(0)$ and $\dot{\varphi}_{1,2}(0)$ at the initial time moment $t=0$], and also on the tilting currents $I_{1,2}$. The current-phase relationship $I_1(\varphi_1)$ for different injection current levels I_2 across the adjacent junction are shown in Figs. 4(b)–4(d). In the insets, the CVC of the junction J_1 is shown schematically for the corresponding I_2 values. If $I_2 = 0$ [see Fig. 4(b); this case corresponds to the experimental curve 3 in Fig. 2], then the $I_1^{\pm}(\varphi_1)$ curves are antisymmetric, $I_1^+(\varphi_1) = -I_1^-(\varphi_1)$, and resemble the current-phase relationship for a single ordinary SIS Josephson junction with the exception that the critical current I_{c1} is lower than that expected for a SIS junction with the same lateral dimensions and the barrier transparency. The current-phase relationship $I_1^{\pm}(\varphi_1)$ for $I_2 < 0$ is plotted in the main panel of Fig. 4(c). If $I_2 < 0$, then the CVC [schematically shown in the inset of Fig. 4(c)] corresponds to the

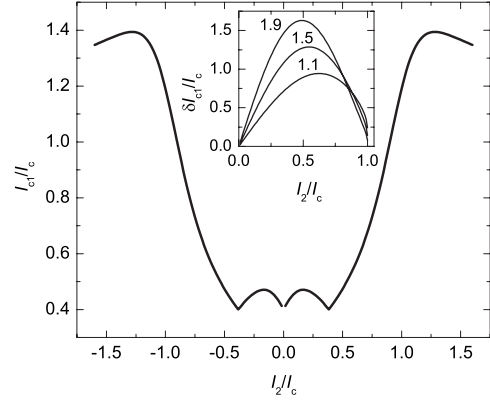


FIG. 5. Main panel: Theoretical dependence of the critical Josephson current of the first SIN subjunction versus the injection current across the second NIS subjunction, $I_{c1}(I_2)$, in the units of the Josephson critical current through the SINIS junction, I_c . Inset: Dependence of the critical current change δI_{c1} as a function of I_2 for $\gamma_J = 1.1, 1.5,$ and 1.9 .

experimental curve 4 in Fig. 2. The upper I_{c1}^+ and lower I_{c1}^- supercurrents are both shifted downward to the region of the negative voltage ($I_{c1}^- < I_{c1}^+ < 0$), similarly to the behavior observed in the experiment (see curve 4 in Fig. 2). At the same time, the magnitude of the partial supercurrent $I_{c1} = I_{c1}^+ + |I_{c1}^-|$ is increased as compared with the corresponding value for $I_2 = 0$. A similar increase of I_{c1} also occurs when the sign of I_2 is reversed, $I_2 > 0$. However, in this case [see Fig. 4(d)], both the upper I_{c1}^+ and lower I_{c1}^- supercurrent values are shifted upward along the current axis, so that the Josephson portion of the CVC may appear completely at positive currents ($I_{c1}^+ > I_{c1}^- > 0$), and some portion of the resistive branch at $I_1 > 0$ appears at $V_1 < 0$ [see the CVC schematically shown in the inset of Fig. 4(d) and the corresponding experimental curve 1 in Fig. 2].

As a mechanical analog of our system, one may consider two pendulums coupled with a spring. In such a system, the interaction renormalizes the eigenfrequencies and alters the oscillation amplitudes of the pendulums, since their equilibrium positions are shifted as compared with those for noninteracting pendulums. In Josephson junction terminology, this corresponds to altering the partial Josephson plasma frequency $\omega_p^{(1,2)} = \sqrt{2eI_{c1,2}/\hbar C_{1,2}}$, where $C_{1,2}$ is the capacitance of either the J_1 or J_2 subjunction. Our quantitative quantum-mechanical model gives a relative increase of the Josephson critical current of the subjunction J_1 , I_{c1} , due to an injection current through the subjunction J_2 , I_2 , as $\delta I_{c1}/I_c = \sqrt{\gamma_J \phi_0^2 / 2\pi} \cdot \exp(-\gamma_J \phi_0^2) / \gamma_J$, where $\gamma_J = \hbar \omega_p^2 / 2eV_J$; here $\phi_0 = \arcsin(I_1 - I_2)$,³ and $V_J = 2e/C = \hbar \omega_p^2 / I_c$ (we assume that the junctions are identical, so that $C_1 = C_2 \equiv C$). From the above expressions one can infer that, in principle, δI_{c1} may exceed I_2 for appropriate SINIS junction parameters.

In Fig. 5 we plot $I_{c1}(I_2)$ in the units of the Josephson critical current of a symmetric SINIS junction, I_c , for the transparency $D = 10^{-5}$ of each subjunction at $T = 0$. The corresponding N-layer thickness was taken to be $d_N = 1.5 \xi_0$ (here

ξ_0 is the BCS coherence length in S); $\omega_p=0.4\Delta$ (here Δ is the superconducting energy gap in S). Comparison of the experimental (cf. Fig. 3) and theoretical (cf. Fig. 5) dependences indicates a good qualitative agreement.

The inset in Fig. 5 shows the theoretical dependence of the change in the Josephson critical current of one junction, δI_{c1} , driven by the injection current I_2 through the other junction, for $\gamma_j=1.1, 1.5$, and 1.9 . One can see that there is a large-signal gain (exceeding 1) for a range of parameters I_2 and γ_j , meaning that, in principle, the device can operate as an amplifier of the Josephson current.

IV. CONCLUSION

We reported an enhancement of the Josephson current in one junction by applying a control current through another junction within the same device. A theoretical model explain-

ing the phenomenon is presented. The supercurrent enhancement described here is a nonlinear effect intrinsic to a SINIS device where the SIN and NIS subjunctions strongly interact by the proximity effect¹⁰ through the N layer; the microscopic mechanism of the interaction is quantum mechanical, rather than electromagnetic¹² in nature, and is related to elementary Andreev reflection processes affected by a local supercurrent.

ACKNOWLEDGMENTS

This work was supported by the National Science Foundation under Grants No. EIA-0218652 and No. DMR-0509357; use was made of facilities operated by the NSF-supported Materials Research Center. One of the authors (S.S.) acknowledges support from AFOSR Grant No. FA9550-06-1-0366.

¹J. E. Nordman, *Supercond. Sci. Technol.* **8**, 681 (1995).

²M. G. Blamire, *Supercond. Sci. Technol.* **19**, S132 (2006).

³S. E. Shafranjuk, *Phys. Rev. B* **74**, 024521 (2006).

⁴I. P. Nevirkovets, O. Chernyashevskyy, J. B. Ketterson, and E. Goldobin, *J. Appl. Phys.* **97**, 123903 (2005).

⁵I. P. Nevirkovets, O. Chernyashevskyy, and J. B. Ketterson, *Phys. Rev. Lett.* **95**, 247008 (2005).

⁶I. P. Nevirkovets, O. Chernyashevskyy, and J. B. Ketterson, *Phys. Rev. B* **73**, 224521 (2006); I. P. Nevirkovets, S. E. Shafranjuk, O. Chernyashevskyy, and J. B. Ketterson, *Phys. Rev. Lett.* **98**, 127002 (2007).

⁷I. P. Nevirkovets, S. E. Shafranjuk, and J. B. Ketterson, *Phys. Rev. B* **68**, 024514 (2003).

⁸O. Kulik, *Zh. Eksp. Teor. Fiz.* **57**, 1745 (1969) [*Sov. Phys. JETP* **30**, 944 (1970)]; C. Ishii, *Prog. Theor. Phys.* **44**, 1525 (1970).

⁹A. Furusaki and M. Tsukada, *Phys. Rev. B* **43**, 10164 (1991); C. W. J. Beenakker and H. van Houten, *Phys. Rev. Lett.* **66**, 3056 (1991).

¹⁰W. L. McMillan, *Phys. Rev.* **175**, 559 (1968).

¹¹T. van Duzer and C. Turner, *Principles of Superconducting Devices and Circuits* (Prentice-Hall, Englewood Cliffs, NJ, 1999).

¹²S. Sakai, P. Bodin, and N. F. Pedersen, *J. Appl. Phys.* **73**, 2411 (1993).

¹³G. Carapella, G. Costabile, R. De Luca, S. Pace, A. Polcari, and C. Soriano, *Physica C* **259**, 349 (1996).